



Fabrication of TiO₂ nanotubes *via* three - electrodes anodization technique under sound waves impact and use in dye-sensitized solar cell

Qahtan A.Yousif * and Noura H. Haran

Department of chemistry, College of science, University of Al-Qadisiyah, Iraq



Abstract

An experimental study on the growth of Titanium dioxide nanotubes (TNTs) during the three-electrode anodization technique of Ti substrate in fluoride-ion /ethylene glycol (EG) electrolyte has been conducted at 20 V for 30 minutes. The evolution of this nanostructure includes the inward growth of a compact porous layer at the oxide/Ti substrate interface that grows into nanotubes. A further explication for the formation of these TNTs via the anodization and ultrasonic vibration techniques were introduced based on the geometric variations observed. X-ray diffraction (XRD) spectrum showed that the dominance of the anatase phase with improved crystallinity properties at crystal size 15.2 nm which was affected by the sound waves. Highly ordered 7.09 μm long TNTs with an average diameter of 65.57 nm were produced in the presence of ultrasound and 4.50 μm long of nanotubes with an average diameter of 51.18 nm were obtained in the absence of ultrasound. Besides, the energy dispersive x-ray (EDX) spectra confirmed the chemical compositions of TiO₂-NTs with an atomic ratio of 1/2 (Ti:O), which indicates the development of TNTs with varying lengths and average diameters. Annealed TiO₂-NTs were applied as photoanode in a back-side illuminated dye-sensitized solar cell. The Full factor, FF of 0.436 (Photoconversion efficiency η , 0.51), was achieved for the TNTs photoanode prepared in the presence of ultrasound higher than DSSC with TNTs photoanode fabricated in the absence of ultrasound.

Keywords: DSSC, Nanotubes, Crystallization, Anodization , and Renewable energy

1. Introduction

Nanostructured titanium dioxide TiO₂ has attracted significant research interest over the latter several decades owing to its possible uses in numerous applications [1] such as [2], supercapacitors[3], photocatalysts[4], and solar cells[5]. The TiO₂ one-dimensional nanostructures can be synthesized by using several techniques, for instance, hydrothermal[6], sol-gel[7], electrospinning[8], freeze-drying[9], and anodization methods[10],[11]. Among these methods, anodization introduces some of the advantages for example control of the dimensions nanostructure, the simple fabrication, and the possibility to synthesis the high ordered TiO₂ nanotubes (TNTs) on the Ti substrate without using the templates[12],[13]. TNTs can be synthesized by the anodization method by using both organic and aqueous electrolytes based on the fluoride ion[14],[15]. Zwilling et al[16]. have reported the

first of nanoporous TiO₂ thin film by the anodization technique. Furthermore, the high ordered of TNTs arrays later synthesized in the hydrofluoride electrolyte by the Gong et al[17]. These studies encouraged a tremendous upsurge of interest in this topic and meaningful adjustments and enhancements of the nanostructure of anodized TiO₂. Furthermore, several studies have been offered of TNTs, Jin Zhang and co-workers[18] have been prepared the TiO₂ nanotubes films via the electrophoretic method on the fluoride doped tin oxide (FTO) glass and study its photovoltaic applications. The porous double-walled TNTs via the ultraviolet- assisted anodization have synthesized by the Ghafar Ali et.al[19]. Kyung and co-workers [20] prepared different nanostructures of TNTs by the hydrothermal method from the industrial materials (P25) on the FTO glass and used as photoanode in dye-sensitized solar cell (DSSCs). In addition, the anodization technique has studied to form TNTs on the Ti foil by several authors[21]–[25]

*Corresponding author e-mail: drqhatanscience@yahoo.com.; (Qahtan A Yousif).

Receive Date: 19 April 2020, Revise Date: 07 August 2020, Accept Date: 20 August 2020

DOI: 10.21608/EJCHEM.2020.28233.2596

©2021 National Information and Documentation Center (NIDOC)

at different voltage values in the various electrolytes via the two electrodes system in the absence of the ultrasound. The dye-sensitized solar cells have received considerable attention in recent years owing to the low cost of energy conversion and easy to use [26]. The researchers on the DSSCs have focused on optimizing the cell components, especially the photoanode (TiO_2) material and the redox electrolyte, which is strongly related to the efficiency of the solar cell [27],[28]. Recently, the fabrication of DSSCs based on the vertical oriented of Titanium dioxide on the Ti foil surface has been extensively utilized in the anodization method in the solar energy scope research [29],[30]. The present work investigates a reliable strategy for fabricating the high order of TiO_2 nanotubes in the presence of ultrasound. The anodization technique was used via a three-electrode system to enhance the control of the internal current passage and reduce the time of the process at a constant voltage of 20 V. The energy conversion assessed after assembling the dye-sensitized solar cell with a counter electrode as graphene nanoplatelets (GNPs).

2: Experiments Details

2:1 Chemical materials

Ammonium fluoride (NH_4F), ethanol ($\text{CH}_3\text{CH}_2\text{OH}$), N3 dye ($\text{C}_{26}\text{H}_{16}\text{N}_6\text{O}_8\text{RuS}_2$), 1-butyl-3-methylimidazolium iodide ($\text{C}_8\text{H}_{15}\text{IN}_2$), lithium iodide (LiI), iodine (I_2), acetonitrile (CH_3CN), ethylene glycol ($\text{C}_2\text{H}_6\text{O}_2$) (EG), Titanium foil (Ti) with high purity attend to 99.7% with thickness 0.25 mm, and Fluorine-doped tin oxide (FTO) with a sheet resistance of $\sim 7 \Omega/\text{square}$ were supplied from the Sigma Aldrich Co. Ltd. Graphene nanoplatelet was purchased from the Supermarket Company, U.S.A. No further purification for the chemical materials that used in the present work.

2:2 Instruments

The instruments that have been used in this study were X-ray diffraction (XRD, Rigaku Miniflex - 600) using a single-wavelength light 1.5104 \AA from source Cu $K\alpha$ with the use of nickel as a filter where the range taken from the angles of deviation (2θ) in this measurement is within the range (10-80) degree, Field-Emission Scanning electron microscope (JEOL JSM -700F type of FE-SEM) at an applied voltages

15.0 Kv with an energy dispersive X-ray spectrometer, DC power supply from Phywe company, ultrasonic bath HS-300 oscillating frequency 40kHz, output of ultrasonic 200W, HP type 3465B digital voltmeter multimeter, and the Keithley 2400 type was supplied from Keithley company to estimate the photocurrent-voltage parameters, and Xenon lamp of the simultaneous intensity of incident light ($100 \text{ mW}/\text{cm}^2$).

3:3 Preparation TiO_2 nanotubes (TNTs)

The electrochemical anodization method was used to prepare the high-order TiO_2 nanotubes on the Ti substrate. The ethylene glycol-based electrolyte containing 1.5 ml H_2O and 0.5 wt% NH_4F was prepared as the electrolyte solution, and a voltage of 20 V was applied in the presence and absence of the ultrasound for 30 min. at 10°C using three electrodes system, as shown in Fig. 1. Besides, a reference electrode was added as a Calomel to control [31] the current values during the anodization process in addition to the counter electrode (Platinum sheet) and the working electrode as a Ti substrate. Before conducting any test, it is necessary to treat the TiO_2 foil in the ultrasonic bath by using acetone and ethanol solvents, and then was rinsed with deionized water and dried with nitrogen steam. The samples were annealed and calcinated at 550°C for 30 min.

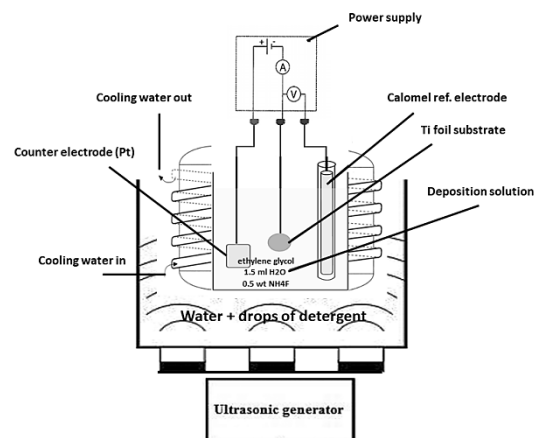


Fig. 1 Components three-electrodes technique.

3:4 Fabrication of NTs -DSSC

Firstly, the graphene nanoplatelet counter electrode was prepared as the same method in our earlier work [31–33]. The TiO_2 -NTs electrode was immersed in N3 dye (1×10^{-4} molar in 20 ml of ethanol and acetonitrile at 40°C) for 24 h after being washed by

water and ethanol and then dried by the nitrogen gas. The electrolyte was prepared by adding some organic additives to increase the stability of electrolytes such as 0.4 M of 1-butyl-3-methylimidazolium iodide as well as 0.1 M of lithium iodide and 0.04 M of iodine. The solar cell is connected to the I-V device after the injection of electrolyte to estimate NTs/GNPs –DSSC parameters

3: Results and Discussion

3:1 XRD Analysis

As shown in **Fig. 2**, the XRD pattern of TiO₂ NTs was prepared in the ethylene glycol electrolyte cantinas of NH₄F and H₂O in the presence and absence of ultrasound after being annealing at 550 °C for 30 min. in the atmospheric oxygen. The anatase phase, which is dominant in the crystal structure of TiO₂ NTs, refers to the crystalline observed after annealing, represented by three strong diffraction peaks that correspond to the diffraction card indexed (*JCPDS 21-1572*). According to the results, the TiO₂ NTs in the presence and absence of ultrasound displayed diffraction peaks at (25.15°, 37.69°, 47.86°), which can be attributed to the (101), (004), (200) anatase crystal faces. Thus, Scherer equation[34] was used to calculate the size of crystalline TiO₂ NTs, and Bragg's equation[35] was utilized to estimate the d-spacing at a specific Miller index (101). The results exhibited the size of the crystal and d-spacing 15.2 nm, 8.48 nm, and 3.53751 nm, 3.53314 nm in the presence and absence of the ultrasound, respectively. It indicates the improved crystallinity at larger crystal size (15.2 nm) of TiO₂ NTs, which was enhanced by an increase in the sharpening of Bragg peaks (101) and intensities. However, it increased the d-spacing (3.53751 nm) value. These results offer evidence of the influence of ultrasound power on the fabrication of Titanium dioxide nanotubes, which is inconsistent with other works[36],[37] when doping the TiO₂-NTs by the heavy metals that leads to confusing the interstitial sites of the TNTs lattice. It is worth to note that the high intensity of the TiO₂-NTs peak reflects the increased length of the nanotube, which is more evident in the ultrasound effect (as we will explain in the FE-SEM section), discrete peaks and papered weak peak at 53.37° (105). Heat treatment at high degrees can significantly increase TiO₂-NT's conductivity. Thus, conductivity is close to 10⁻⁴ μ m⁻¹

for amorphous titanium dioxide nanotubes and about 10⁻⁹ μ m⁻¹ for its crystalline structure [38].

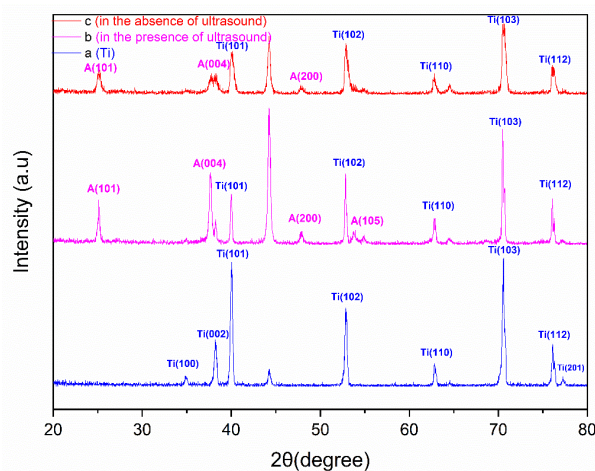


Fig. 2 XRD for the standard diffraction pattern (a) and annealed TNT/Ti arrays in the presence and (b) in the absence of ultrasound (c)

3:2 FE-SEM/AFM observations

It is imperative to take and analyze FE-SEM images to understand the formation of TiO₂ nanotubes. **Fig. (3a to 3g)** reveal that the Titanium dioxide nanotubes grew directly on Ti foil after the anodization in the ethylene glycol electrolyte solution that contains NH₄F and H₂O in the absence and presence of ultrasound. It was observed that the fabrication nanotubes were irregular and ordered in a high dense via the intersection crossing of the structure of tubes that is slightly unclear. It is difficult to obtain a smooth surface to precipitate the excessive water and high anodizing voltage, as suggested by researchers[39],[40]. These precipitates need to be removed from the TiO₂ surface electrode before I-V measurements to facilitate the chemical adsorption of N3 dye for impregnation inside the nanotubes by the electrolyte. Thus, the cross-section exhibits that TiO₂-NTs have a length of 4.50 μm and a tube diameter of 17.36 nm without the ultrasound waves and a length of 7.09 μm and a tube diameter of 21.24 nm in the presence of ultrasound. It seems that wall thickness was slightly thicker in the presence of ultrasound. **Fig. 3 (d) and (h)** show the quantitative analysis of the EDX spectra and chemical compositions of TiO₂-NTs. It can be seen that the main elements were titanium and oxygen, and the atomic ratio of Ti to O was equal to the stoichiometry

of 1/2, indicating that nanotubes were obtained with varying lengths and average diameters.

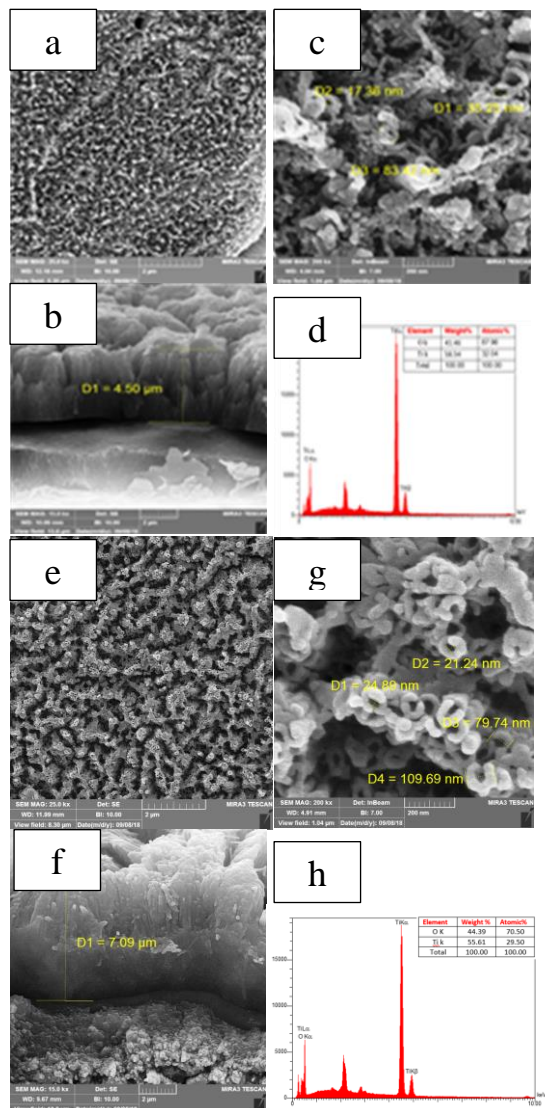


Fig. 3 SEM images of TiO₂-NTs arrays (a,e) top view (scale bar= 2μm; (c,g) pore diameter, (b,f) cross-sectional view, and (d,h) EDX spectra in the absence and presence of ultrasound waves, respectively.

AFM is a technique commonly used to identify the nature of the surface structure and its average thickness. Hence, as shown in Table (1) and **Fig. 4**, in the AFM analysis of the main factors for the description of surface topography, including mean roughness (Ra), root mean square roughness (Rq), the third factor is the surface Skewness, which is denoted by (Rsk). It is used to measure the distribution of the heights and dips of the surface morphology. The

negative value indicates that dips are more abundant than the heights, and the positive value indicates the opposite, which is characterized by an asymmetric structure. The fourth factor is surface Kurtosis (R_{ku}), which can have three values. A value of 3 means that data distribution is followed Gaussian curve, which is called Mesokurtic. A value of less than 3 means that the surface is plane, which is called Platykurtic, and values larger than three reveal that there are more peaks than dips, which is called leptokurtic[22]. As shown in **Table (1)**, R_{ku} below 3 indicates a surface in both cases despite the slight change. Rq and Ra values are lower owing to the ultrasound effect on the fabrication of the TiO₂ nanotubes, which is consistent with a thickness value of 18.53 nm, as shown in

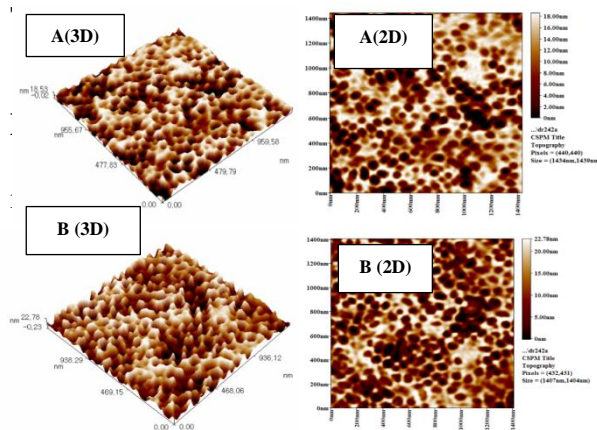


Fig. 4 : Two- and three-dimensional AFM images of TiO₂ nanotubes (A) in the presence of ultrasound and (B). in the absence of ultrasound.

3:3 Mechanism of TNTs and its performance in the DSSC.

As shown in **Fig.5**, the current density versus time curve of the transient response observed during the anodization process in the (EG/ NH₄F / H₂O) electrolyte in the presence and absence of ultrasound waves.

It is exhibited in three different sections of the porous oxide layer. At the beginning of the anodizing process and in the presence of ultrasound, a rapid the current intensity drops rapidly to the lowest value due to high resistance to the oxide layer and ions movements such as O⁻², OH⁻, Ti⁺⁴, and F⁻¹.

Table 1: The statistical roughness coefficients of samples prepared (A) in the presence and (B) in the absence of ultrasound

Vertical distance	R _q	R _{sk}	R _{Ku}	R _a (nm)	Thickness (nm)	Amplitude Factors
2.10	4.83	-0.311	1.92	5.61	18.53	A
1.51	5.80	-0.007	1.79	6.68	22.78	B

The high-resistance barrier layer is necessary to maintain the process of oxidation. Hence, in the presence of fluoride ions, the oxide layer (first section) is drilled and the current suddenly rises to the maximum value, leading to the growth of porosity. This will reduce resistance of the layer barrier (second section). When the current reaches a steady-state, the titanium dioxide nanotube (third section) is formed. The classical interpretation owing to the speed of oxide formation at the metal /oxide interface is equivalent to the rate of decay at the oxide/electrolyte interface[41].

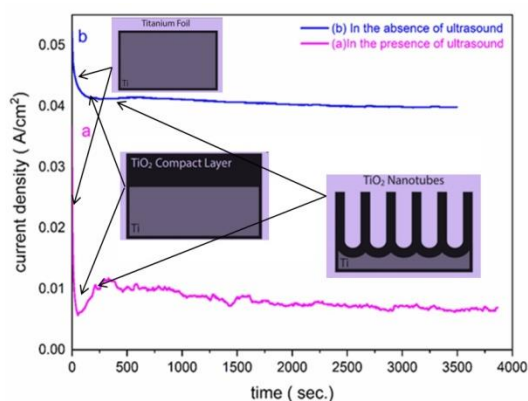


Fig. 5 Current density – time curve of anodized Ti at 20 V for 30 min. (a) in the presence of ultrasound (b) and in the absence of ultrasound in ethylene glycol electrolyte solution of NH₄F and H₂O

It has been displayed the increase in the total charge density corresponds to the rise in fluoride concentration. What can be concluded from the said points is that the anodization voltage is one of the most significant parameters pertaining to the TiO₂ nanotube arrays and the morphology of surface electrode also influence the ultrasound waves, as shown in **Fig. 5**, when compared to curves that describe the fabrication steps of nanotubes. In other words, the curve at the third section remains unchanged and enhances the growth porous on the compact oxide layer in the absence of ultrasound. It is due to retarding the fluoride anion migration towards the Ti electrode in the electrolyte solution. Nevertheless, the anions mobility has accelerated by the sound vibration to promote the growth progress of NTs-TiO₂ in highly ordered and oriented

perpendicularly on the Titanium substrate and enhanced the wall thickness of NTs-TiO₂-Ns. These explanations were corresponding with FE-SEM images analyzed as aforementioned. Based on these observations, 20 V appears to strikes the fit balance with the use of ultrasound waves, which reduces fabrication time to 30 min.

Fig. 6 and **Table (2)** display the electrical parameters of the dye-sensitized solar cell. The excellent conversion efficiency was observed in the presence of ultrasound compared to its absence. It uses the graphene nanoplatelets which is coated on the FTO glass as the counter electrode.

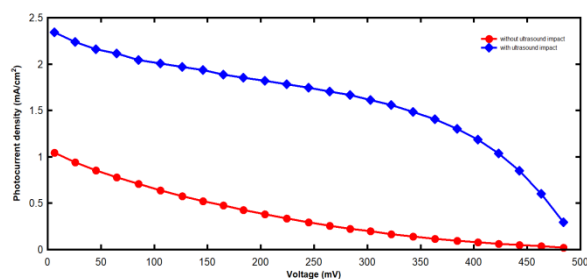


Fig. 6: J-V curves of NTs/GNPs–DSSC in the ethylene glycol electrolyte in NH₄F and H₂O (a) in the presence of ultrasound and (b) in the absence of ultrasound at simulated sunlight (100 mW/cm²)

The low values of the short circuit current are related to the high resistance of FTO glass substrate coated by graphene nanoplatelets, which are consistent with the series resistance values, as shown in **Table 2**, as well the nature of nanotubes in adsorbing the dye molecules when compared to a film of TiO₂ nanoparticles. Furthermore, the photocurrent-voltage parameters such as open circuit voltage (V_{oc}), short circuit current density (J_{sc}), voltage at max power point (V_{mpp}), current at max power point (I_{mpp}), fill factor (FF) and cell conversion efficiency (η) as well series resistance (R_s) and shunt resistance were estimated from the J-V curves, as depicted in **Table 2**.

Table 2: Photocurrent – voltage parameters of dye-sensitized NTs/GNPs–DSSC at simulated sunlight (100 mW/cm²)

Electrolyte (anodization voltage and time)	Length (μm)	Diameter (nm)	J _{sc} (mA/cm ²)	V _{oc} (V)	FF	Refs.
EG/NH ₄ F/H ₂ O (60 V for 12 h) ^b	18	100	7.2	0.65	0.45	[42]
EG/DMSO (60 V for 18 h) ^b	10	150	3.2	0.65	0.55	
EG/NH ₄ F/HF (120 V for 2 h) ^b	18	150	3.1	0.63	0.62	[43]
EG/HF (120 V for 2 h) ^b	20	-	7.8	0.65	0.46	[44]
EG/NH ₄ F/H ₂ O (60 V for 1 h) ^b	10	150	7.1	0.64	0.53	
EG/1.5mL H ₂ O/0.5wt% NH ₄ F (20 V for 30 min.) in the absence of ultrasound	4.50	51.18	1.040	0.518	0.144 ^a	
EG/1.5mL H ₂ O/0.5wt% NH ₄ F (20 V for 30 min.) in the presence of ultrasound	7.09	65.57	2.336	0.500	0.436 ^a	This work

^a For the FF 0.144 and 0.436, the η equal to 0.08 and 0.51, respectively. ^b This refers to the use of the two-electrodes system without the ultrasound.

The synthesis of TiO₂ nanotubes in the presence of ultrasound waves to fabricate the NTs/GNPs–DSSC demonstrated improved performance compared to other photoelectrode, with an overall conversion efficiency of 0.510 to enhance attributes of the conduction band[38]. Photocurrents can be affected by the charge transfer, electrons injection rate, and charge recombination process. Thus, the electron injection rate depends on the position of LUMO in the dye molecules as well as the conduction band of TiO₂ NT[45]. It was appeared to be a perfect match between dye molecules (LUMO) and the conduction band of TiO₂ NTs that reinforce the rate of electron injection and so the overall DSSC efficiency is more accurate. The impact of ultrasound on the open-circuit potential was also observed, and hence (V_{oc}) value dropped in TiO₂ TN electrode due to its association with the conduction band edge[46] of Titanium dioxide nanotubes.

4: Conclusion

In this work, Titanium dioxide nanotubes (TNTs) arrays on Ti substrates were successfully fabricated during the anodization technique by using three electrodes system at a constant voltage of 20 V for 30 min in the ethylene glycol electrolyte cantinas of NH₄F and H₂O in the presence and the absence of ultrasound. It was found that the XRD measurements were confirmed the dominant Anatase phase with high purity in corresponding with (101), (004), and (200) Miller indexes. Furthermore, the results have indicated the improved crystallinity at a large crystal size (15.2 nm) of TNTs that enhanced by an increase in the intensity peak of (101). FESEM images showed the

formation highly ordered of TNTs arrays of (7.09 μm) and (4.50 μm) lengths with the average diameters of (65.57 nm) and (51.18 nm) with and without ultrasound, respectively. AFM results reinforced the FESEM data when the Rq and Ra values have lowered due to the ultrasound effect on the fabrication of TNTs and corresponding with the thickness value of 18.53nm. In addition, the DSSCs based on the as-prepared TNTs were fabricated and investigated. So, TNTs films are appropriate to severe as the photoanodes of DSSCs, the best full factor of energy conversion efficiency of the DSSCs achieves 0.436 under simulated sunlight of 100 mW/cm².

Funding

The present research received no external funding.

Conflict of Interests

The two authors declare no conflict of interests, financial or otherwise

5: References

1. Yang, Y., Li, Y. & Pritzker, M. Morphological evolution of anodic TiO₂ nanotubes. *RSC Adv.* **4**, 35833–35843 (2014).
2. Zhang, Q. *et al.* CuO nanostructures: Synthesis, characterization, growth mechanisms, fundamental properties, and applications. *Prog. Mater. Sci.* **60**, 208–237 (2014).
3. Zhang, G. *et al.* Enhanced charge storage by the electrocatalytic effect of anodic TiO₂ nanotubes. *Nanoscale* **3**, 4174–4181 (2011).
4. Tatarchuk, T., Peter, A., Al-Najar, B., Vijaya, J. & Bououdina, M. Photocatalysis: Activity of Nanomaterials. *Nanotechnol. Environ. Sci.* **1–2**, 209–292 (2018).
5. Han, Y. S. & Kim, J. T. Enhanced Performance

- of Dye-Sensitized Solar Cells with Surface-treated Titanium Dioxides. *Mol. Cryst. Liq. Cryst.* **565**, 138–146 (2012).
6. Liao, J. Y., Lei, B. X., Chen, H. Y., Kuang, D. Bin & Su, C. Y. Oriented hierarchical single crystalline anatase TiO₂ nanowire arrays on Ti-foil substrate for efficient flexible dye-sensitized solar cells. *Energy Environ. Sci.* **5**, 5750–5757 (2012).
 7. Yan, F. D. *et al.* Photovoltaic Performance Enhancement in Dye-Sensitized Solar Cells with Periodic Surface Relief Structures. *J. Macromol. Sci. Part a-Pure Appl. Chem.* **46**, 1213–1216 (2009).
 8. Hamadani, M. & Jabbari, V. Fabrication and characterization of dye-sensitized solar cells using electrospun TiO₂ nanofibre as a solar light harvesting layer. *Int. J. Sustain. Energy* **31**, 277–289 (2012).
 9. Shafae, M., Goharshadi, E. K., Mashreghi, M. & Sadeghinia, M. TiO₂ nanoparticles and TiO₂@graphene quantum dots nanocomposites as effective visible/solar light photocatalysts. *J. Photochem. Photobiol. A Chem.* **357**, 90–102 (2018).
 10. Smith, Y. R., Sarma, B., Mohanty, S. K. & Misra, M. Light-assisted anodized TiO₂ nanotube arrays. *ACS Appl. Mater. Interfaces* **4**, 5883–90 (2012).
 11. Tenkyong, T. *et al.* Structural modulation and band gap optimisation of electrochemically anodized TiO₂ nanotubes. *Mater. Sci. Semicond. Process.* **83**, 150–158 (2018).
 12. Guan, D. & Wang, Y. Synthesis and growth mechanism of multilayer TiO₂ nanotube arrays. *Nanoscale* **4**, 2968 (2012).
 13. Zhang, Q., Wang, H.-Y., Jia, X., Liu, B. & Yang, Y. One-dimensional metal oxide nanostructures for heterogeneous catalysis. *Nanoscale* **5**, 7175–83 (2013).
 14. Regonini, D., Bowen, C. R., Jaroenworarluck, A. & Stevens, R. A review of growth mechanism, structure and crystallinity of anodized TiO₂ nanotubes. *Mater. Sci. Eng. R Reports* **74**, 377–406 (2013).
 15. Shankar, K. *et al.* Highly-ordered TiO₂ nanotube arrays up to 220 μm in length: Use in water photoelectrolysis and dye-sensitized solar cells. *Nanotechnology* **18**, (2007).
 16. Zwilling, V. *et al.* Structure and Physicochemistry of Anodic Oxide Films on Titanium and TA6V Alloy. *Surf. Interface Anal.* **27**, 629–637 (1999).
 17. Gong, J., Lin, C., Ye, M. & Lai, Y. Enhanced photoelectrochemical activities of a nanocomposite film with a bamboo leaf-like structured TiO₂ layer on TiO₂ nanotube arrays. *Chem. Commun. (Camb)*. **47**, 2598–2600 (2011).
 18. Zhang, J., Li, S., Yang, P., Que, W. & Liu, W. Deposition of transparent TiO₂ nanotubes-films via electrophoretic technique for photovoltaic applications. *Sci. China Mater.* **58**, 785–790 (2015).
 19. Ali, G., Kim, H. J., Kim, J. J. & Cho, S. O. Controlled fabrication of porous double-walled TiO₂ nanotubes via ultraviolet-assisted anodization. *Nanoscale* **0–5** (2014) doi:10.1039/c3nr05894h.
 20. Sun, K. C., Qadir, M. B. & Jeong, S. H. Hydrothermal synthesis of TiO₂ nanotubes and their application as an over-layer for dye-sensitized solar cells. *RSC Adv.* **4**, 23223–23230 (2014).
 21. Nyein, N., Tan, W. K., Kawamura, G., Matsuda, A. & Lockman, Z. TiO₂ nanotube arrays formation in fluoride/ethylene glycol electrolyte containing LiOH or KOH as photoanode for dye-sensitized solar cell. *J. Photochem. Photobiol. A Chem.* **343**, 33–39 (2017).
 22. Bozkurt Çırak, B. *et al.* Synthesis, surface properties, crystal structure and dye sensitized solar cell performance of TiO₂ nanotube arrays anodized under different voltages. *Vacuum* **144**, 183–189 (2017).
 23. Chanmanee, W. *et al.* Formation and Characterization of Self-Organized TiO₂ Nanotube Arrays by Pulse Anodization. *J. Am. Chem. Soc.* **130**, 965–974 (2008).
 24. Di Yao, D., Field, M. R., O'Mullane, A. P., Kalantar-Zadeh, K. & Ou, J. Z. Electrochromic properties of TiO₂ nanotubes coated with electrodeposited MoO₃. *Nanoscale* **5**, 10353–10359 (2013).
 25. Lin, L. Y. *et al.* Highly ordered TiO₂ nanotube stamps on Ti foils: Synthesis and application for all flexible dye-sensitized solar cells. *Electrochem. commun.* **37**, 71–75 (2013).
 26. Chandrasekaran, S. *et al.* Recent advances in metal sulfides: From controlled fabrication to electrocatalytic, photocatalytic and photoelectrochemical water splitting and beyond. *Chem. Soc. Rev.* **48**, 4178–4280 (2019).

27. Deka, J. R. & Wang, H. W. Rapid Synthesis of Mesoporous TiO₂ for the Photoanodes in Dye Sensitized Solar Cells. *J. Chinese Chem. Soc.* **61**, 1049–1055 (2014).
28. Yousif, Q. A. & Agbolaghi, S. A Comparison Between Functions of Carbon Nanotube and Reduced Graphene Oxide and Respective Ameliorated Derivatives in Perovskite Solar Cells. *Macromol. Res.* 20–21 (2019) doi:10.1007/s13233-020-8054-8.
29. Ahmad, A., Yerlikaya, G., Zia-ur-Rehman, Paksoy, H. & Kardaş, G. Enhanced photoelectrochemical water splitting using gadolinium doped titanium dioxide nanorod array photoanodes. *Int. J. Hydrogen Energy* **45**, 2709–2719 (2020).
30. Nie, X. *et al.* Synthesis and characterization of TiO₂ nanotube photoanode and its application in photoelectrocatalytic degradation of model environmental pharmaceuticals. *J. Chem. Technol. Biotechnol.* **88**, 1488–1497 (2013).
31. Haran, N. H. & Yousif, Q. A. The efficiency of TiO₂ nanotube photoanode with graphene nanoplatelets as counter electrode for a dye-sensitized solar cell. *Int. J. Ambient Energy* **0**, 1–14 (2019).
32. Yousif, Q. A. & Haran, N. H. Fabrication and Characterization of TiO₂ Nanowires as Photoanode Electrode of the Dye-Sensitized Solar Cell. *J. Comput. Theor. Nanosci.* **16**, 3013–3017 (2019).
33. Haran, N. H. & Yousif, Q. A. Characterization and Fabrication of nanowires as a photoanode electrode for DSSC. *J. Phys. Conf. Ser.* **1294**, (2019).
34. Patterson, A. L. The scherrer formula for X-ray particle size determination. *Phys. Rev.* **56**, 978–982 (1939).
35. El-Sayed, H. a & Birss, V. I. Controlled growth and monitoring of tantalum oxide nanostructures. *Nanoscale* **2**, 793–8 (2010).
36. Ma, X., Sun, Z. & Hu, X. Synthesis of tin and molybdenum co-doped TiO₂ nanotube arrays for the photoelectrocatalytic oxidation of phenol in aqueous solution. *Mater. Sci. Semicond. Process.* **85**, 150–159 (2018).
37. Subramanian, A. & Wang, H. W. Effects of boron doping in TiO₂ nanotubes and the performance of dye-sensitized solar cells. *Appl. Surf. Sci.* **258**, 6479–6484 (2012).
38. Wang, H. *et al.* Nitrogen-doped TiO₂ nanoparticles better TiO₂ nanotube array photoanodes for dye sensitized solar cells. *Electrochim. Acta* **137**, 744–750 (2014).
39. González, J. R. *et al.* Long-Length Titania Nanotubes Obtained by High-Voltage Anodization and High-Intensity Ultrasonication for Superior Capacity Electrode. *J. Phys. Chem. C* **116**, 20182–20190 (2012).
40. Tian, J., Zhao, Z., Kumar, A., Boughton, R. I. & Liu, H. Recent progress in design, synthesis, and applications of one-dimensional TiO₂ nanostructured surface heterostructures: A review. *Chem. Soc. Rev.* **43**, 6920–6937 (2014).
41. Motlak, M., Hamza, A. M., Hammed, M. G. & Barakat, N. A. M. Cd-doped TiO₂ nanofibers as effective working electrode for the dye sensitized solar cells. *Mater. Lett.* **246**, 206–209 (2019).
42. Hwang, H. Y., Prabu, A. A., Kim, D. Y. & Kim, K. J. Influence of the organic electrolyte and anodization conditions on the preparation of well-aligned TiO₂ nanotube arrays in dye-sensitized solar cells. *Sol. Energy* **85**, 1551–1559 (2011).
43. Hu, X. *et al.* Fabrication of carbon-modified TiO₂ nanotube arrays and their photocatalytic activity. *Mater. Lett.* **62**, 4579–4581 (2008).
44. Jennings, J. R., Ghicov, A., Peter, L. M., Schmuki, P. & Walker, A. B. Dye-Sensitized Solar Cells Based on Oriented TiO₂ Nanotube Arrays: Transport, Trapping, and Transfer of Electrons. 13364–13372 (2008).
45. Kwok, E. C. H., Chan, M. Y., Wong, K. M. C. & Yam, V. W. W. Molecular dyads comprising metalloporphyrin and alkynylplatinum(ii) polypyridine terminal groups for use as a sensitizer in dye-sensitized solar cells. *Chem. - A Eur. J.* **20**, 3142–3153 (2014).
46. Suhaimi, S., Shahimin, M. M., Alahmed, Z. A., Chyský, J. & Reshak, A. H. Materials for Enhanced Dye-sensitized Solar Cell Performance: Electrochemical Application. **10**, 2859–2871 (2015).